行政院國家科學委員會補助專題研究計畫 □成果報告 ■期末報告

混合式火箭前瞻推進次系統發展及空氣動力優化研究與發展(二年)

Development of an Advanced Propulsion Subsystem and Aerodynamics Optimization for a Hybrid Rocket **(2 Years)**

計畫類別：■個別型計畫　□整合型計畫
計畫編號：NSC-99-2221-E-009-056-MY2
執行期間： 99 年 08 月 01 日至 101 年 07 月 31 日

執行機構及系所：國立交通大學機械工程學系

計畫主持人：吳宗信
共同主持人：黃俊誠、陳彥升
計畫參與人員：胡孟樺、周子豪、莊康旻、林哲緯、楊奇融

成果報告類型(依經費核定清單規定繳交)：■精簡報告　□完整報告

本計畫除繳交成果報告外，另須繳交以下出國心得報告：
□赴國外出差或研習心得報告
□赴大陸地區出差或研習心得報告
□出席國際學術會議心得報告
□國際合作研究計畫國外研究報告

處理方式：除列管計畫及下列情形者外，得立即公開查詢
　　　　　■涉及專利或其他智慧財產權，□一年■二年後可公開查詢

中　華　民　國 100 年 5 月 31 日

行政院國家科學委員會專題研究計畫期末報告

混合式火箭前瞻推進次系統發展及空氣動力優化研究與發展(二年)

Development of an Advanced Propulsion Subsystem and Aerodynamics Optimization for a Hybrid Rocket **(2 Years)**

計畫編號：NSC-99-2221-E-009-056-MY2

執行期限：99 年 08 月 01 日至 101 年 07 月 31 日

主持人：吳宗信　國立交通大學機械工程學系

共同主持人：黃俊誠(國立海洋大學)、陳彥升（財團法人國家實驗研究院）

計畫參與人員：胡孟樺、周子豪、莊康旻、林哲緯、楊奇融

中文摘要

近年來，混合式火箭的研究已經在世界各地的引起極大的關注。主要是因為它具有高度安全性，綠色推進特性和良好的比衝值(例如，N_2O 及 HTPB 最佳組合:~250)，因此其研發成本與其它如固態或液態火箭推進方式相對低廉許多。其中混合式推進次系統仍然是最重要的次系統之一，因其優劣直接決定火箭大部份的性能。在此計畫中我們選擇了商業上易取得的 N_2O 與 HTPB 分別當作氧化劑與燃料。此外，空氣動力的優化對一個火箭系統發展是一樣重要的。本期末報告書描述本計畫二年來研發的結果: 1)完成推力約 300 kgf 混合式火箭推進次系統的地面測試(內含混合增強器、單節與單流道設計)，地面比衝值 218。2)透過平行 2D、3D 計算流體力學進行模擬混合式冷流場與燃燒因渦旋群集增強器所造成複雜反應流現象與推力增強。3)同時利用 component building up model 來建立具尾翼結構(單節設計火箭)的氣動力資料庫。

關鍵字: 混合式火箭推進、計算流體力學、燃燒、氣動力學

Abstract

Recently, hybrid rocket research has attracted tremendous attention for several research institutes around the world, mainly because of its inherited high degree of safety, simplicity, green propulsion and good ISP, which results in relatively low development cost. Nevertheless, the hybrid propulsion subsystem is still one of the most important subsystems, which determines the rocket's performance in general. Since nitrous oxide is self-pressurized, unlike LOX or others that requires complicated cryogenic pumping system, we have chosen commercially available nitrous oxide and HTPB as the oxidizer and fuel, respectively, in the proposed study. In addition, aerodynamics optimization of a rocket is also important subject, which is addressed in this proposed subproject. Thus, in this final report, we report our progress of this project in the 2-year period. Firstly, we have successfully developed a single-stage, single-port hybrid propulsion subsystem with a mixing enhancer for ground and real flight test with thrust of ~300 kgf. Secondly, we have explored preliminarily the complex cold and reacting flow phenomena caused by the patented vortex clustering mixing enhancer through parallel 2D, 3D CFD simulations. Thirdly, we have also built up the aerodynamics database for fin-body configuration (single stage) using component building up model.

Keywords: hybrid rocket propulsion, computational fluid dynamics, combustion, aerodynamics.

1. Introduction

Hybrid rocket propulsion applies both solid and liquid as the propellants, instead of solids or liquids. In a typical hybrid rocket system, the mixing of the liquid oxidizer with solid fuel is controlled by an oxidizer valve between their storage tank and chamber, respectively. Albeit some similarity exists between hybrid rocket and solid or liquid rocket, the principles of operation is totally different. In solid and liquid rockets, both fuel and oxidizer are premixed with approximately the same O/F ratio (mass ratio of oxidizer to fuel). However, the O/F ratio in a hybrid rocket varies with the location and time in the combustion port. In addition, the combustion in a hybrid combustor is in the form of turbulent diffusion flame, in which the combustion efficiency is not as good as turbulent premixed flame in general.

As compared to other two kinds of rocket (solid and liquid), the technology of hybrid rocket is still under developing and requires tremendous effort to make it become a useful sounding rocket or even satellite launcher in the space industry. However, it represents one of the attractive alternatives to solid and liquid rockets. Major motivation of interest comes from the many advantages as compared to them. The hybrid rocket is a propulsion system which combines the solid and liquid propulsion systems. It includes about half of the plumbing system of the liquid rocket, which keeps its flexibility of thrust control intact; while it avoids the highly explosive characteristics of the solid rocket. In brief, the advantages include: 1) simplicity, 2) safety, 3) performance, 4) environmental friendly and 5) cost [1-2].

However, in addition to the above mentioned advantages, the hybrid rocket also possesses some disadvantages which are summarized as follows. They include: **1**) lower regression rate (~1 mm/s) due to characteristics of diffusion flame, **2**) multi-port combustor which reduces the bulk volumetric density and possibly requires the web support for grain integrity, **3**) lower combustion efficiency because of diffusion flame, **4**) variation of O/F ratio depending on the position and time in the combustion port, **5**) low-frequency instabilities causing the large thrust variation during the flight and **6**) slower response of the flow rate control. One thing about the low-frequency instabilities is that it may be caused by either the injection system or the easy de-bonding paraffin fuel as promoted by the group of Prof. Cantwell of Stanford University. Nevertheless, these could be possibly leveraged or resolved through proper researches. But one of the most important principles, in resolving these disadvantages, is that the solution cannot reduce the simplicity, safety and cost advantages of the hybrid rocket system. Otherwise, it is not worthy of conducting such kind of research in essence.

Thus, the objectives of this project are to thoroughly study the fundamental and practical aspects of hybrid N2O-HTPB propulsion and optimization of aerodynamics related to a real rocket system. However, because NSC only grants 2 years for this project, instead of 3 years, as proposed originally, several of the objectives might have to be adjusted due to limited resources of time and budget.

The present final report is organized as follows. Experimental and numerical methods are introduced briefly in Section 2. Section 3 presents the preliminary results and related discussion. In Section 4, the conclusions of the present study are summarized along with several future directions of research. Finally, Appendix I presents **國科會補助專題研究計畫成果報告自評表.**

.

2. Research Methods

2.1 Numerical Method for Cold and Reacting Flow for Hybrid Motor

The CFD methodology is based on a multi-dimensional, finite-volume, viscous, chemically reacting, unstructured grid, and pressure-based formulation. Time-varying transport equations of continuity, species continuity, momentum, total enthalpy, turbulent kinetic energy, and turbulent kinetic energy dissipation were solved using a time-marching sub-iteration scheme and are written as:

$$\frac{\partial \rho}{\partial t}+\frac{\partial}{\partial x_j}\left(\rho u_j\right)=0 \tag{1}$$

$$\frac{\partial \rho\alpha_i}{\partial t}+\frac{\partial}{\partial x_j}\left(\rho u_j\alpha_j\right)=\frac{\partial}{\partial x_j}\left[\left(\rho D+\frac{\mu_t}{\sigma_\alpha}\right)\frac{\partial \alpha_i}{\partial x_j}\right]+\omega_i \tag{2}$$

$$\frac{\partial \rho u_i}{\partial t}+\frac{\partial}{\partial x_j}\left(\rho u_j u_i\right)=-\frac{\partial p}{\partial x_i}+\frac{\partial \tau_{ij}}{\partial x_j} \tag{3}$$

$$\frac{\partial \rho H}{\partial t}+\frac{\partial}{\partial x_j}\left(\rho u_j H\right)=\frac{\partial p}{\partial t}+Q_r+\frac{\partial}{\partial x_j}\left(\left(\frac{K}{C_p}+\frac{\mu_t}{\sigma_H}\right)\nabla H\right)+\frac{\partial}{\partial x_j}\left(\left((\mu+\mu_t)-\left(\frac{K}{C_p}+\frac{\mu_t}{\sigma_H}\right)\right)\nabla\left(V^2/2\right)\right)+\theta \tag{4}$$

$$\frac{\partial \rho k}{\partial t}+\frac{\partial}{\partial x_j}\left(\rho u_j k\right)=\frac{\partial}{\partial x_j}\left[\left(\mu+\frac{\mu_t}{\sigma_k}\right)\frac{\partial k}{\partial x_j}\right]+\rho(\Pi-\varepsilon) \tag{5}$$

$$\frac{\partial \rho\varepsilon}{\partial t}+\frac{\partial}{\partial x_j}\left(\rho u_j\varepsilon\right)=\frac{\partial}{\partial x_j}\left[\left(\mu+\frac{\mu_t}{\sigma_\varepsilon}\right)\frac{\partial \varepsilon}{\partial x_j}\right]+\rho\frac{\varepsilon}{k}\left(C_1\Pi-C_2\varepsilon+C_3\Pi^2/\varepsilon\right) \tag{6}$$

A predictor plus corrector solution algorithm was employed to provide coupling of the governing equations. A second-order central-difference scheme was employed to discretize the diffusion fluxes and source terms. For the convective terms, a second-order upwind total variation diminishing difference scheme was used. To enhance the temporal accuracy, a second-order backward difference scheme was employed to discretize the temporal terms. Details of the numerical algorithm can be found in Ref's [3-9].

An extended k-ε turbulence model [10] was used to describe the turbulence. A modified wall function approach was employed to provide wall boundary layer solutions that are less sensitive to the near-wall grid spacing. Consequently, the model has combined the advantages of both the integrated-to-the-wall approach and the conventional law-of-the-wall approach by incorporating a complete velocity profile and a universal temperature profile [11]. A finite-rate chemistry chemical reaction mechanism [12-18] was used to describe the combustion process occurs inside the hybrid combustion chamber.

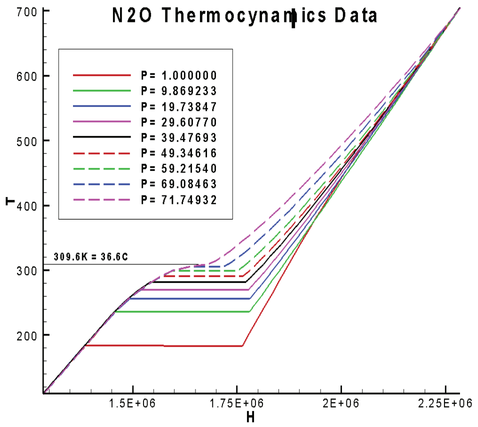

Figure 1 N2O thermodynamic data.

In order to make analyses of phase change phenomena commonly occurs in combustion devices such as cavitation, liquid sprays and/or cryogenic fluid flows, real-fluid thermal and caloric equations of state (EOS) were developed for use with the present CFD code. The HBMS equations of state [19-21] were chosen for this purpose. Thermal and caloric equations of state, vapor pressure, heat of vaporization, surface tension, and transport properties are modeled with the equations of state proposed by Hirshfelder, et al [22] (we term these the HBMS equations of state) and with conventional correlations [23], for the other properties. The property correlations used were not chosen for their absolute accuracy, but for their validity over a wide range of temperatures and pressures and for requiring a minimum of data to describe a particular species. These correlations are explicit in density and temperature. These equations are not only of sufficiently high order that properties are accurately predicted for a wide range of conditions, but component submodels may be easily modified. In this instance, the vapor pressure curve and the liquid phase density correlations were improved over the original HBMS formulations. Other equations of state were considered, but were found to be not as satisfactory as the HBMS equations. **Figure 1** shows the phase diagram of N2O.

Multi-component mixtures were treated, by adding partial specific volumes or pressures. The partial volume methodology is essential to improve the accuracy of the prediction when a small amount of multi-component vapor and a large amount of liquid are present at the same point. The fluid property routines also include correlations for the transport properties.

In practical implementation, a real-fluid HBMS model based on a time-saving look-up table is used following a recently published book by one of the co-PIs (Dr. Yen-Sen Chen) [24]

In the present numerical investigation, N2O/HTPB combustion conditions are of interest. A reduced 12-species and 16-step reaction chemical kinetics mechanism [25] is employed for the combustion simulation. Note HTPB is simplified as C4H6 since it constitutes major part of the HTPB.

2.2 Numerical Method for Aerodynamic Design Analysis

Component Build-up Method for Aerodynamics Database

The component build-up method (CBM) is a combination of theoretical, semi-empirical and semi-analytic techniques. This method is a balance between configuration applicability, accuracy, and usage cost. The component build-up method of DATCOM developed by USAF has been proven to produce acceptable preliminary missile and rocket design accuracy for more than 80% of the configurations and flight conditions examined [26-27]. We will employ this CBM to build up the database for rocket aerodynamic configuration design as required in the proposed study, which are described as follows.

The CBM separates the rocket aerodynamic coefficients into the summation of related components. For example, the overall lift coefficient can be written as (e.g., single stage, body-fin configuration)

$CN = CNb + CNf + CNfb + CNbf$

where CNb is normal force coefficient of body alone, CNf is normal force coefficient of fins alone, CNbf is the body normal force coefficient increment due to the interference of fins, and CNfb is the fin normal force coefficient increment due to the interference of body. In this study, we will employ the method proposed in Jorgensen [28] and Pitts et al. [29] to calculate CNb. Their method is based on drag coefficients obtained from the two dimensional cylinder to build up a set of correction formulas. This is used to modify the results by the slender body potential flow theory and specially useful for subsonic, transonic and supersonic aerodynamics prediction. In current study, CNf will be interpolated from a series charts created by the aerodynamics simulation code, xFlow, which will be used to simulate a series of single fin and construct the table for aerodynamic coefficients. Considered geometry includes leading edge sweep angle, aspect ratio, tap ratio and fin section, among others. Fin cross section includes: 1) double wedge and 2) modify double wedge. According to the theory of equivalent angle of attack [30-31], CNfb and CNbf can be written as

$CNfb = Kf \times CNb \qquad CNbf = Kb \times CNf$

where Kf and Kb is the interference coefficient of wing and body, respectively. In this proposed study, we will design several versions of standard wing-body configuration and apply xFlow code to calculate wing-body interference for validation. Based on this, we can then build up the coefficients Kf and Kb.

Similarly, pitch moment coefficient can be written as

$Cm = Cmb + Cmf + Cmfb + Cmbf$

Similar treatment can be applied to calculate this coefficient. As for the drag coefficient, it can be written as

$CD = CD0 + CDi$

Note CDi is proportional to the square of AOA. CD0 is the sum of CD0b and CD0f. These two parts come from the contributions of nose cone pressure drag, friction drag and base drag. We will calculate the nose cone pressure drag based on [29] for different flow regimes. Friction drag will be calculated using Van Driest II formula [32]. Base drag will be calculated based empirical chart [33-34].

Aerodynamics Design for Single Fin-Body Configuration

In the 1st year, we will design a fin-body configuration for rocket system. In addition to the diameter that is determined by the size of the motor and avionic subsystem, the other important parameters, including the length of the nose, the length of the rocket (3-4 m), skirt, stabilized fins and geometrical parameter of the wing section, leading edge sweep angle, aspect ratio, tape ratio, will be decided based on the proposed method.

The idea of designing aerodynamic configuration in the 1st year include: 1) Large fineness ratio of body to reduce the wave drag during supersonic flight, which may increase the starting AOA for boundary layer separation in the leeward side because of weaker viscous cross flow effect during the subsonic flight; 2) Tapered plan form of medium aspect-ratio wing (1-2) with modified double wedge fin, which can benefit the flight stability and fin structure loading, especially the limit of the bending moment; and 3) Pre-rolling incidence angle (intentionally tilted) for fin to increase the flight stability.

2.3 Experimental Methods

Figure 2 shows the schematic diagram of the thrust test stand we used at the test site of NCTU. The maximum thrust for this system is 500 kgf. For the test, the motor is placed horizontally on the test stand with load cell at the end of the sliding table. Test N2O tank is hanged at the top to reduce the friction on the rail of the platform. There are two simple ball valves between the N2O tank and the pintle injector. One is located just right at the exit of the N2O tank, which is manually controlled for safety; while the other is located prior to the injector and is controlled by either pneumatic cylinder or stepper motor. Note through several previous tests, we have found that this stepper motor control valve (in-house designed and made via gear reduction as shown in **Figure 3**) can be fully open within ~1 second.

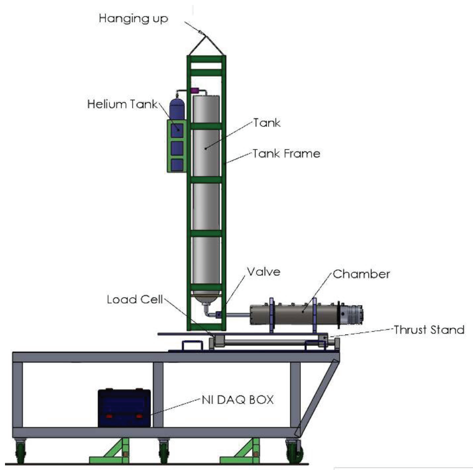

Figure 2 Schematic diagram of the planned static-burn test configuration of the hybrid combustion.

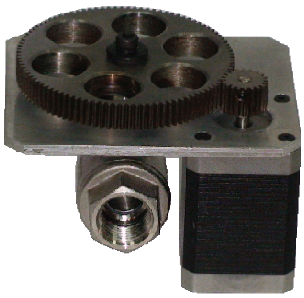

Figure 3 In-house designed valve control module using stepper motor and a gear set.

Figure 4 Previous hybrid combustion chamber (left) and mounted on the test stand

High pressure transducers are used to measure the instantaneous pressure of N2O vapor in the N2O tank and hybrid combustion chamber (both pre- and post-). K-type thermocouples are used to measure the instantaneous surface temperature of N2O tank and the temperatures at various positions at the surface of the motor chamber. All the above sensors and signal control for on/off of the valves are connected to a data acquisition system (cDAQ 9172, National Instruments Inc.) and then the data are output into a laptop computer. The DAQ software was programmed using LabView libraries. In addition, **Figure 4** shows a photo of hybrid combustion chamber made of stainless steel mounted on the test stand.

3. Results and Discussion

3.1 Cold Flow Simulation of Hybrid Motor with a Mixing Enhancer

Figure 5 shows the sketch of model hybrid motor with a mixing enhancer positioned at the inlet of single port. **Figure 6** shows an explosive view of the grids near the mixing enhancer used for CFD modeling. In order to simplify the grid generation and reduce the total number of cells, I-blanking method was used to generate the mesh of vane, although this may not follow the exact geometry of the vane, which we think it will influence the overall structure the flow field too much.

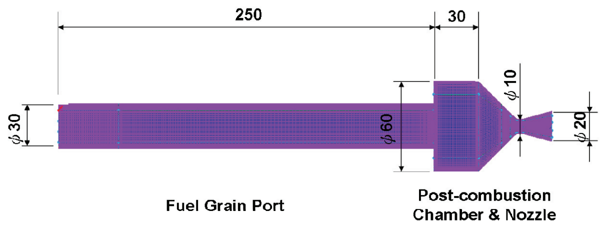

Figure 5 Geometry of a model hybrid motor with a mixing enhancer at the inlet of the single port.

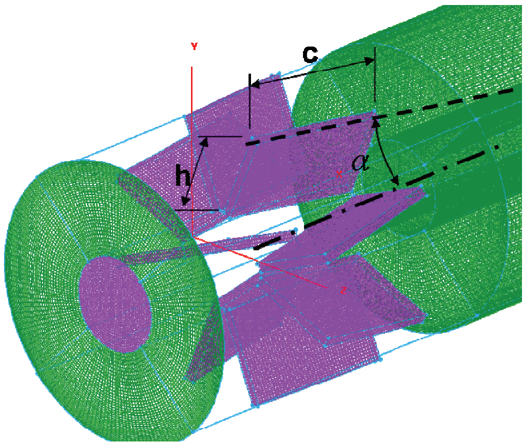

Figure 6 The clustered mixing enhancer near the inlet of the single port. Chord length (c), van height (h), and angle of attack (α).

To characterize the mixing in the combustion port due to the clustered mixing enhancer following earlier study [35], we calculate the average of magnitude of axial vorticity (ω_x) as

$$\omega_{x,avg} = \frac{\iint_{port} abs(\omega_x)\cdot dA}{A_{port}}.$$

In addition, ratio of transverse to streamwise kinetic energy following the earlier study [36] is also computed as

$$R_{T-S} = \frac{\int_A (V^2 + W^2)\rho}{\int_A U^2 \rho}$$

In the present study, we have employed different number of vanes (4, 6 and 8) and results of Mach number distribution at various locations behind the vanes are shown in **Figure 7**.

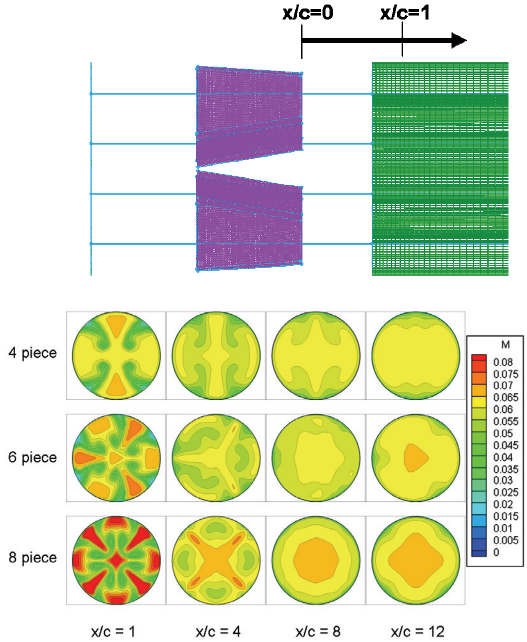

Figure 7 Distributions of Mach number at different axial locations behind the clustered vanes for various numbers of vanes.

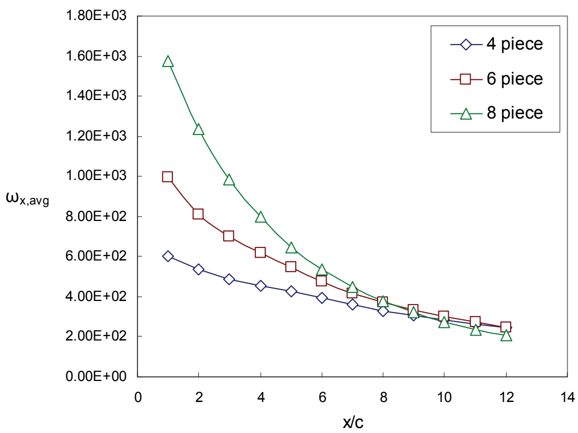

Figure 8 Average magnitude of axial vorticity at various locations with different number of vanes.

Figure 8 shows the average magnitude of axial vorticity at various locations with different number of vanes. Results show that vorticity generated by the clustered vanes increases with increases with increasing number of vanes, especially in the near wake field behind the vanes. For example, the vorticity generated by 8 pieces is about 2.7 times as compared that by 4 pieces right after the vanes. This will promote the mixing of N2O and vaporized HTPB in a real hybrid motor. **Figure 9** shows similar trend of Ratio of transverse to streamwise kinetic energy at various locations with different number of vanes.

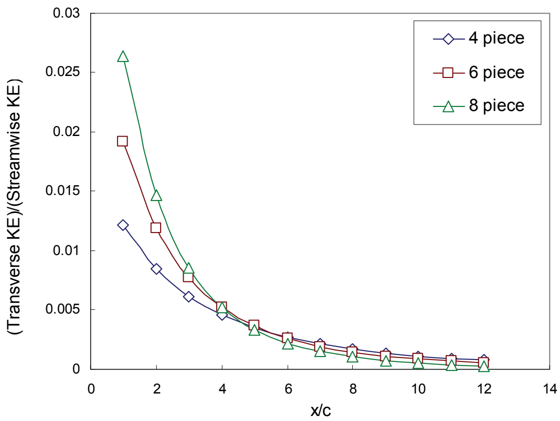

Figure 9 Ratio of transverse to streamwise kinetic energy at various locations with different number of vanes.

By taking the advantage of symmetry, we only take 1/8 of original port for production run (Figure 10). Note that we have also performed a full-scale simulation to make sure this simplification is appropriate.

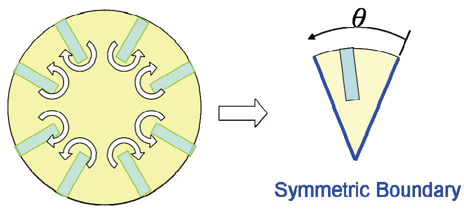

Figure 10 Symmetric boundary condition in 1/8 cylinder.

Because the limited space in the port space, change of span, chord length and angle of attacked are constrained. We decided to fix one parameter then change different combinations of another two. Figure 11 & Figure 12 show the averaged axial vorticity magnitude and ratio of kinetic energy at different locations behind the blade tip. In this case we fix chord length as 15 mm with different combinations of span and angles of attack. Results show that the combination of span of 6 mm in length and angle of attack of 23.5° has the best performance (highest vorticity). Figure 13 shows the streamline of flow field using the optimum geometry of blades. We can see the decay of vorticity after blade is very fast. That also implies we need 2 stage mixing enhancer to sustain the enhanced vorticiy.

Figure 14(a) shows the axial velocity gradient with respect to radial direction (dU_x/dR) at the port surface using the combination of best performance as mentioned in the above. Results show that there exists very large positive value at the blade tips and very large negative value right behind the blade that is caused by a reversed flow structure. Figure 14(b) shows the distribution of azimuthal velocity gradient (dU_θ/dR) with respect to radial position. We can see the peak value that is smaller than that those presented in Figure 14(a) appearing on the tip at the downside. We expect those downstream regions at the solid fuel surface behind the large axial velocity gradients would be burned faster with a larger regression rate. Figure 15 shows that observed burned HTPB fuel surface behind a mixing enhancer with eight blades. It clearly shows the experimental pattern strongly correlates with what we have found from the numerical simulation.

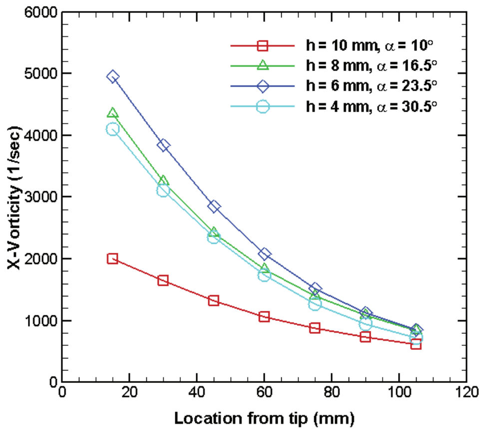

Figure 11 Axial vorticity magnitude with fixed chord length (15 mm) and different combination of span & angle of attack.

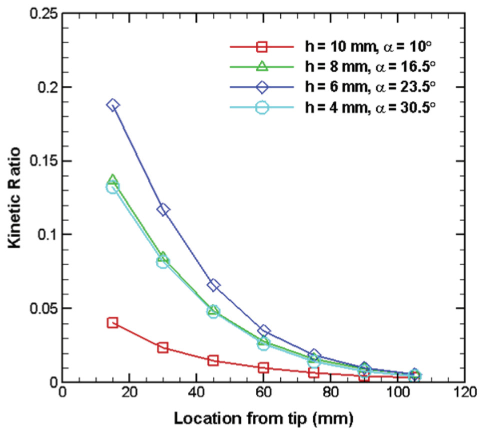

Figure 12 Ratio of transverse to streamwise kinetic energy with fixed chord length (15 mm) and different combination of span & angle of attack.

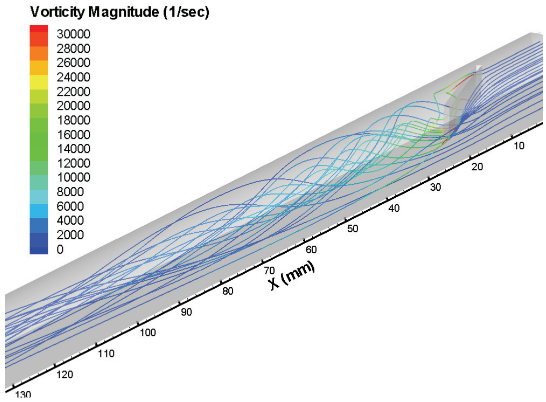

Figure 13 Streamline & vorticity magnitude of 1/8 chamber cold flow simulation.

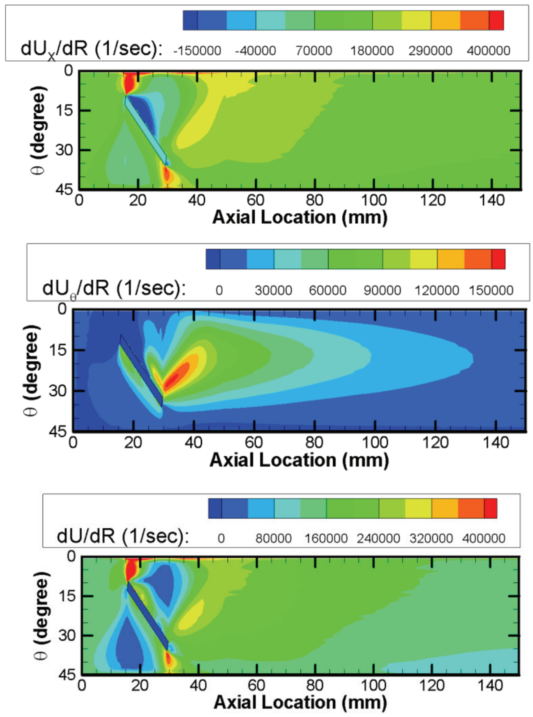

Figure 14 (a) Axial velocity gradient distribution, and (b) azimuthal velocity gradient distribution on port surface.

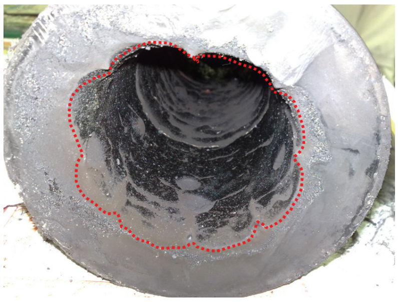

Figure 15 The burned fuel surface just after mixing enhancer.

3.2 Reacting Flow Simulation of Hybrid Motor with a Mixing Enhancer

Figure 10 shows a series of simulation data for axisymmetric configuration without including the clustered mixing enhancer at the port inlet. Results show that even for this axisymmetric CFD simulation gas flows are oscillating when reaching quasi-steady state. This can also be clearly observed in the temporal thrust curve as shown in Figure 11. High temperature regions as high as 3,000 K occur close to the HTPB surface because this is a typical diffusion flame. In the pre-combustion chamber, temperatures are as high as 3,000 K, which requires vey careful thermal insulation in practice to prevent the chamber from melting down. Also the use of the simple Pintle injector has led to a very cold region around the injector head because of self-cooling caused by the flow field. This has been further proved in our static-burn tests that the Pintle injector was intact after burning more than 20 seconds. However, large fraction of oxygen is exhausted directly throughout the nozzle without burning because of low combustion efficiency of a typical diffusion flame with weak mixing between fuel and oxidizer. In addition, only a small amount of NO is generated which shows that the N2O-HTPB hybrid combustion is a green propulsion technology, unlike solid-propellant such as AP (ammonia perchrola), which releases poisonous HCl that is highly poisonous.

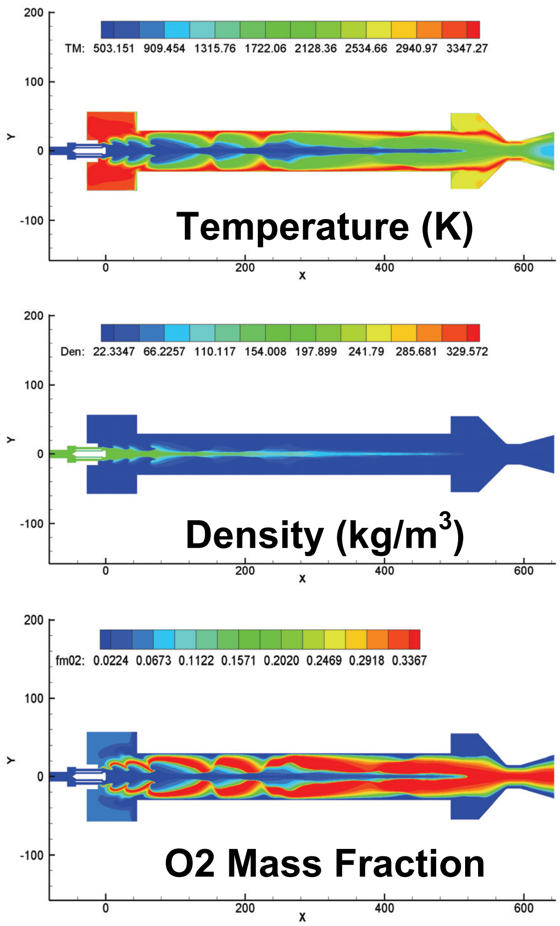

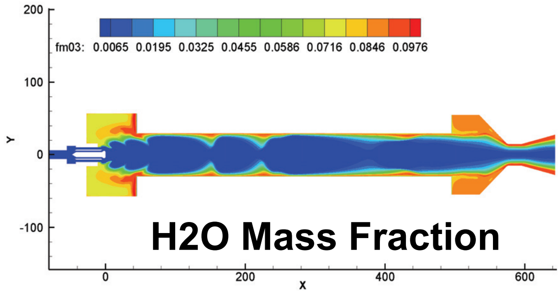

Figure 10 Distributions of flow properties of an axisymmetric simulation of a N2O-HTPB hybrid motor.

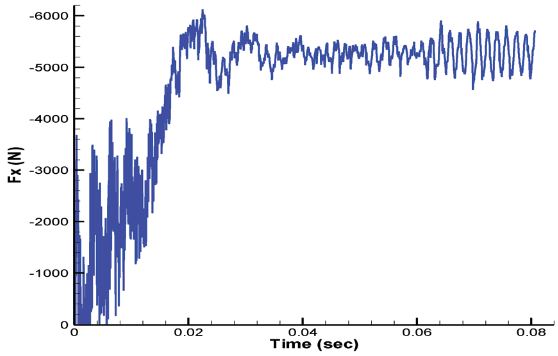

Figure 11 Simulated temporal thrust curve.

Figure 12 shows the comparison of the instantaneous temperature between the 3D simulations (~5 million cells using 128 processors of an IBM-1350 PC cluster at NCHC) with and without the clustered mixing enhancer. Results show that mixing is clearly enhanced by positioning a clustered mixing enhancer near the port inlet. In addition, the 3D simulations again confirm that the cold region behind the Pintle injector as found in the earlier mentioned axisymmetric simulations.

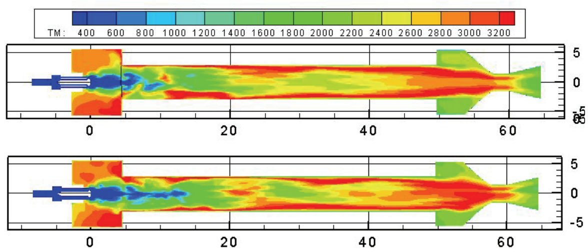

Figure 12 the comparison of the temperature between the 3D simulations (~5 million cells using 128 processors of an IBM-1350 PC cluster at NCHC) with (top) and without (bottom) the clustered mixing enhancer.

Figure 13 shows the 3D simulation results of 1/8 combustion chamber of HTTP-2 beta hybrid rocket with different setups of mixing enhancers. We can see the typical diffusion flame occurs in the chamber without mixing enhancer, and the flame in the chamber with a mixing enhancer has been disturbed obviously. The flame is more homogeneous at end part of chamber in the chamber with 2-stage mixing enhancer (both have the same angle of attack).

Table 1 summarizes the important results from different arrangements of mixing enhancers. Obviously, the chambers with mixing enhancer(s) have the better ISP because of better combustion efficiency that means less propellant is needed to generate the same chamber pressure. Higher combustion efficiency also increases the chamber pressure that leads to decrease of the mass flow rate of oxidizer (N2O). It results in decrease of O/F ratio and becomes more close to stoichiometric ratio.

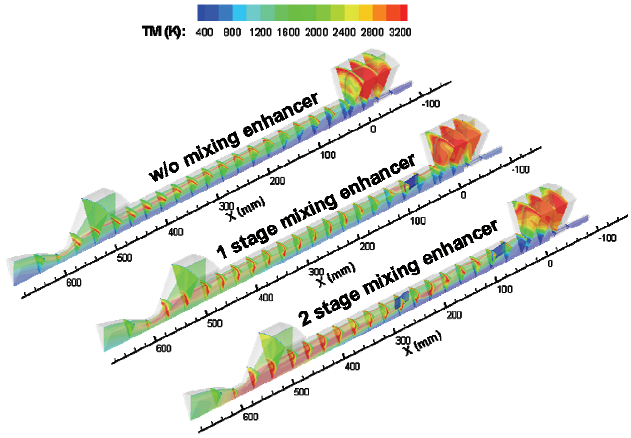

Figure 13 Temperature distribution of 1/8 symmetric simulation of N2O-HTPB hybrid motor with different types of mixing enhancers.

Table 1 Performance of N2O-HTPB hybrid motor simulations with different setup of mixing enhancer.

Enhancer Type	w/o	Single Stage	2 Stage (opposite angle)	2 stage (same angle)
Chamber Pressure (bar)	27.12	27.36	29.12	29.16
Total Mass Flow Rate (kg/sec)	1.61	1.42	1.36	1.31
N2O Mass Flow Rate (kg/sec)	1.48	1.26	1.20	1.15
HTPB Mass Flow Rate (kg/sec)	0.14	0.16	0.17	0.16
O/F Ratio	10.87	7.92	7.17	7.21
Thrust Force (kgf)	331.84	332.83	331.80	332.62
ISP (sec)	205.9	234.9	251.1	254.8

3.3 Aerodynamic Design Analysis

We have designed a single fin-body configuration for rocket system. In addition to the diameter that is determined by the size of the motor (15 cm), the nose length (40 cm) and the length of rocket (2.5-3.5 m), the other important parameters, including stabilized fins and geometrical parameter of the wing section, leading edge sweep angle, aspect ratio, tape ratio, were decided based on the proposed method. The idea of designing aerodynamic configuration include: 1) Large fineness ratio of body to reduce the wave drag during supersonic flight, which may increase the starting AOA for boundary layer separation in the leeward side because of weaker viscous cross flow effect during the subsonic flight; 2) Tapered plan form of medium aspect-ratio wing (1-2) with modified double wedge fin, which can benefit the flight stability and fin structure loading, especially the limit of the bending moment; and 3) Pre-rolling incidence angle (intentionally tilted) for fin to increase the flight stability.

Figure 13 shows the two different designs of the rocket, and the total lengths are 250 cm and 350, respectively. Both designs used the same wing section configuration: length of fin root is 30 cm, length of fin tip is 10 cm and semi fin span is 10 cm. **Figure 14** shows the plane dimensions of three different designs of rocket. **Figure 15** shows the zero angle of attack drag coefficient with Mach number. **Figure 16** shows the zero angle of attack lift coefficient varies with Mach number, in which the lift coefficient shows significant difference from subsonic region to transonic region. In subsonic region, longer rocket also increases the lift coefficient. In the transonic region, lift coefficient doesn't correlate well with the rocket length. **Figure 17** shows the zero angle of attack pitching moment coefficient varies with Mach number. In subsonic region, longer rocket length will also increase the pitching moment coefficient. In the region of supersonic flight, the pitching moment coefficient is not proportional to the rocket length. Since centre of pressure move back, the pitching coefficient derivatively increase.

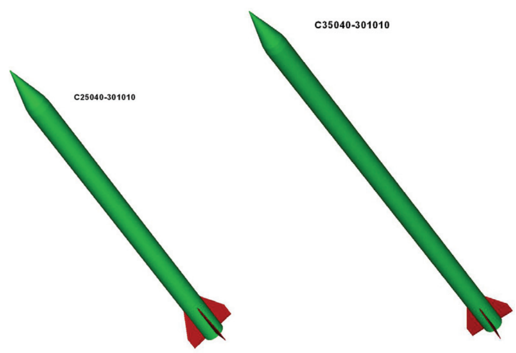

Figure 13 Two different designs of rocket. Left: 2.5 m; right: 3.5 m.

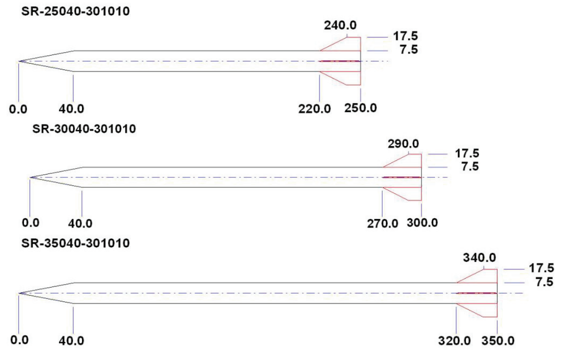

Figure 14 The dimensions of three different designs of rocket.

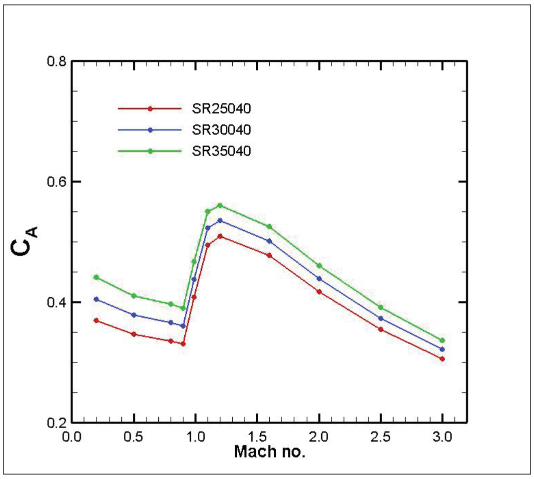

Figure 15 The zero angle of attack drag coefficient with Mach number.

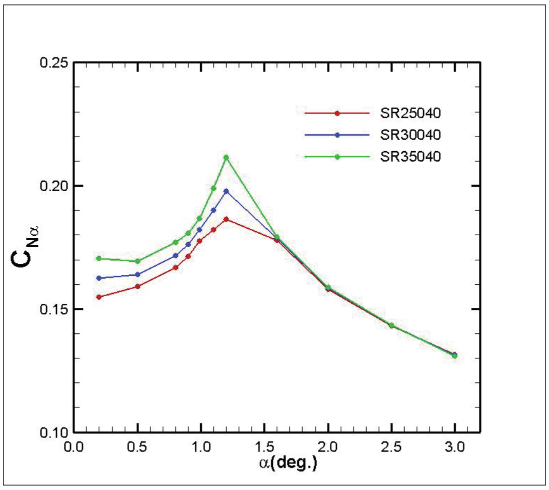

Figure 16 The zero angle of lift coefficient with Mach number.

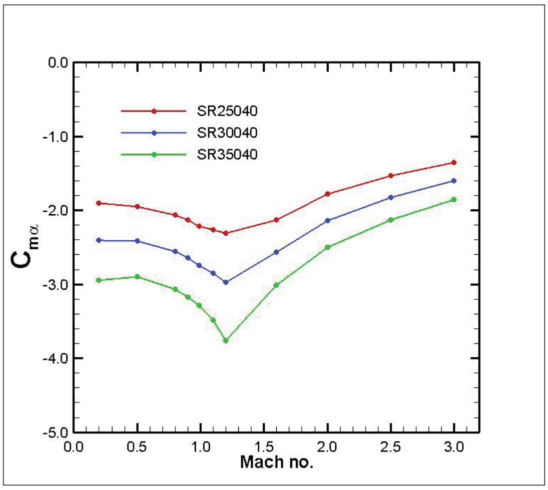

Figure 17 The zero angle of pitching moment coefficient with Mach number

3.4 Static-Burn Tests

We have conducted five times of large-scale static-burn tests. One typical result is shown in **Figure 18**. Results show that this hybrid motor can produce thrust more than 300 kgf for 6.5 seconds continuously simply by self-pressurization of N2O in the tank. Rapid decrease of the thrust, and thus the tank pressure, after 6.5 seconds of burning is simply because the N2O liquid has fully gasified.

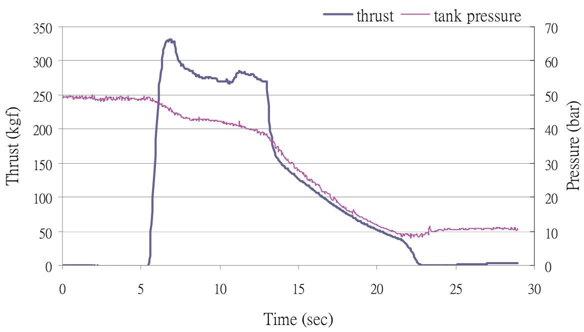

Figure 18 Thrust and N_2O tank pressure of the static burn test data of HTTP-1 hybrid motor.

3.5 Venturi flow meter for mass flow rate measurement

To realize thrust control in the future, we need an accurate flow meter for the flight computer to control the flow rate of oxidizer flowing into the combustion chamber. Three different venturi flow tubes, including 10, 28 and 28 mm in inlet diameter with 8, 16 and 20 mm in throat diameter were designed to cover different ranges of mass flow rates, including 1~2, 3~8, 6~12 kg/s, respectively. A venturi flow meter calibration system for pressurized nitrous oxide or carbon dioxide is developed and validated by comparing between experiments and simulations.

Figure 21 shows the simulation results of geometric design of venturi. Results show that there are no cavitations occur when liquid gas flow passes it, and the resulting pressure loss is very low. Incompressible Bernoulli type empirical correlation that links between pressure difference (inlet and throat) and mass flow rate is written as:

$$\dot{m}_{ox} = C_v A_2 \sqrt{\frac{2\rho_{ox}\Delta P}{1-(\frac{A_2}{A_1})^2}}$$

where A_1 and A_2 are the inlet area and throat area respectively. ΔP is the pressure difference between inlet and throat, ρ_{ox} is the density of oxidizer, and Cv is velocity coefficient. Figure 22 shows the velocity coefficient for the venturi flow meter is 0.96, 0.97 and 0.91 for mass flow rate range 1~2, 3~8, 6~12 kg/s, respectively.

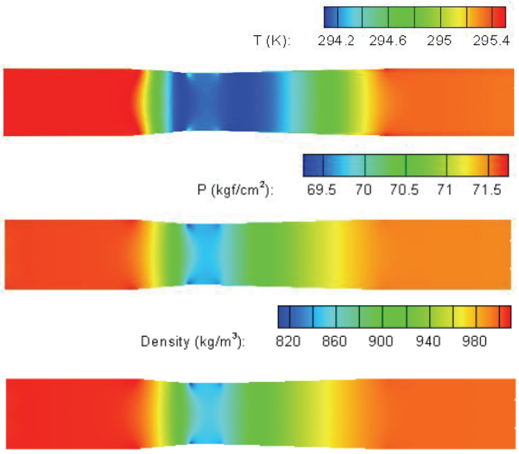

Figure 21 Simulated flow properties of nitrous oxide in the Venturi flow meter (D=28 mm and d=24 mm).

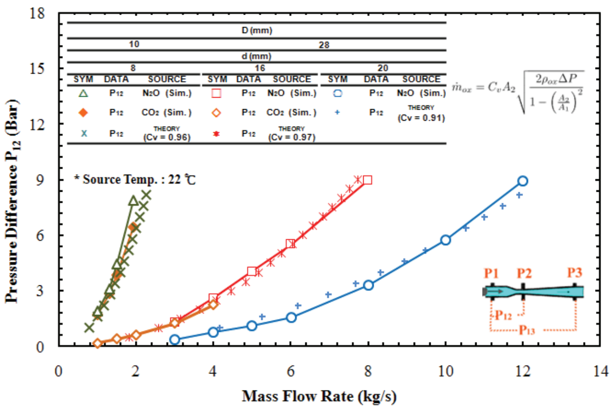

Figure 22 Overall simulation results in comparison with Bernoulli eqn. theory results

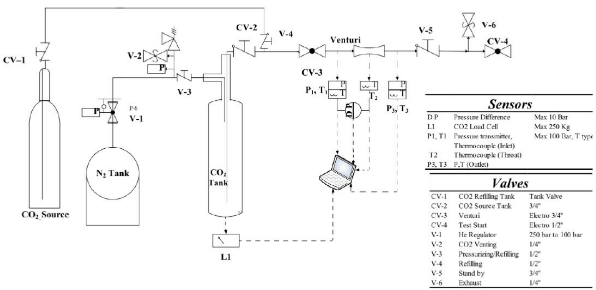

Figure 23 Schematic diagram of venturi flow meter calibration system.

Figure 23 shows the venturi flow meter calibration system, includes a nitrogen pressurized source tank with adjustable pressure, a venturi flow tube and an orifice. Different tank pressures, with or without an orifice at downstream, are used to change the flow rate. Solenoid valves and pneumatic ball valves are used with extended electrical wires which every socket has independent switch, that we can do the experiments by remote control. CO2 is used as the working gas in this study instead of N2O because of their similarity in thermodynamic behavior and also large cost saving.

Pressure transducers, differential pressure transducer (Figure 24) and thermocouples are used to measure instantaneous pressure and temperature. A load cell is used to measure the instantaneous weight of the pressurized tank during experiments that can be used to deduce the instantaneous mass flow rate. These data are collected by a data acquisition system (NI 9205, NI9213 and NI cDAQ-9172) and a personal computer.

Figure 24 The venturi flow meter with pressure transducers used in the experiments.

Comparison of simulation and experimentsare shown in Figures 25 and 26. The simulations agree very well with the measurements. Velocity coefficients of empirical correlation based on the Bernoulli equation is fitted to be 0.96 for the flow rates as mentioned in the above.

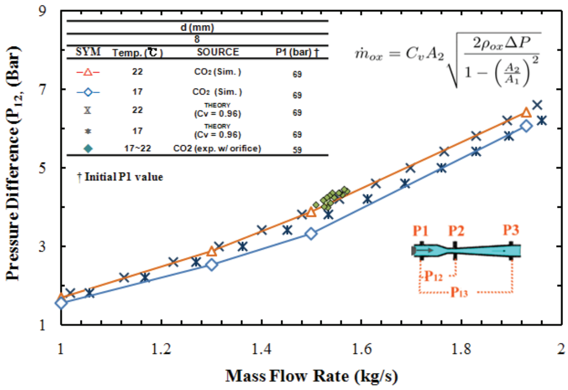

Figure 25 Empirical correlation for venturi diameter 10 mm and different temperature.

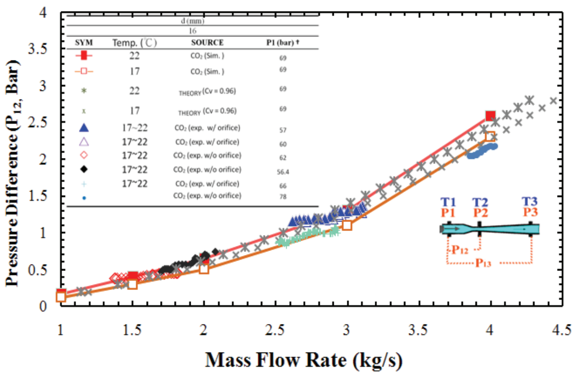

Figure 26 Empirical correlation for venturi diameter 28 mm and different temperature.

4. Conclusion

In this final report, we have presented what we have performed in the past two years:

1. Complex 2D and 3D parallel CFD simulations for cold and reacting flows in a hybrid N2O-HTPB were performed. Results show that vorticity behind the clustered mixing enhancer increases with increasing number of vanes. In addition, they also show that large portion of oxygen is exhausted out through the nozzle without burning. Temperature in the pre-combustion chamber is as high as 3,000K, which requires special care in thermal insulation in practice. Also the design of a simple Pintle injector ensures ensure a cold flow region behind the head that prevents it from being melted down.

2. Based on 3D CFD simulations, ISP increases with increasing stages of mixing enhancers in the port because of enhanced mixing between fuel and oxidizer in the port.

3. Aerodynamic design analysis is completed for a single stage rocket with different lengths.

4. Static burn tests showed that the designed N2O-HTPB hybrid motor can produce more than 300 kgf of thrust.

References

1. Karabeyoglu, A., Seminar of Aero/Astro 50th Year Anniversary, SPG Inc., Department of Aeronautics and Astronautics, Stanford University, May 9, 2008.
2. Chiaverini M.I. and Kuo K.K., Fundamentals of Hybrid Rocket Combustion and Propulsion, Vol. 218, Progress in Astronautics and Aeronautics, 2007.
3. Wang, T.S., Chen, Y.S., “Unified Navier-Stokes Flowfield and Performance Analysis of Liquid Rocket Engines,” J. Propulsion and Power, Vol. 9, No. 5, pp. 678-685, 1993.
4. Chen, Y.-S., Liu, J., Zhang, S., and Mallapragada, P., “An Integrated Tool for Launch Vehicle Base-Heating Analysis,” Final Report, NAS8-00002, Engineering Sciences, Inc., Huntsville, AL, 2001.
5. Liaw, P., Shang, H.M., Chen, Y.S., “Particulate Multi-Phase Flowfield Calculation with Combustion/Breakup Models for Solid Rocket Motor,” AIAA-94-2780, 30th AIAA/ASME/SAE/ASEE Joint Propulsion Conference, June 27-29, 1994, Indianapolis, IN.
6. Chen. Y.-S., Zhang S., and Liu, J., “Stage Separation Performance Analysis Project,” Final Report, H-34345D, Engineering Sciences, Inc., Huntsville, AL, 2002.
7. Wang, T.-S., Chen, Y.-S., Liu, J., Myrabo, L.N., and Mead, F.B. Jr., “Advanced Performance Modeling of Experimental Laser Lightcraft,” Journal of Propulsion and Power, Vol. 18, No. 6, 2002, pp. 1129-1138.
8. Wang, T.-S., “Multidimensional Unstructured-Grid Liquid Rocket Engine Nozzle Performance and Heat Transfer Analysis,” Journal of Propulsion and Power, Vol. 22, No. 1, 2005, pp. 78-84.
9. Wang, T.-S., “Transient 3-D Analysis of Nozzle Side Load in Regeneratively Cooled Engines,” AIAA Paper 2005-3942, 41st AIAA/ASME/SAE/ASEE Joint Propulsion Conference, Tucson, Arizona, 2005.
10. Chen, Y.-S., and Kim, S. W., “Computation of Turbulent Flows Using an Extended k-ε Turbulence Closure Model,” NASA CR-179204, 1987.
11. Wang, T.-S., “Multidimensional Unstructured-Grid Liquid Rocket Engine Nozzle Performance and Heat Transfer Analysis,” Journal of Propulsion and Power, Vol. 22, No. 1, 2005, pp. 78-84.
12. Liaw, P., Shang, H.M., Chen, Y.S., “Particulate Multi-Phase Flowfield Calculation with Combustion/Breakup Models for Solid Rocket Motor,” AIAA-94-2780, 30th AIAA/ASME/SAE/ASEE Joint Propulsion Conference, June 27-29, 1994, Indianapolis, IN.
13. Chen. Y.-S., Zhang S., and Liu, J., “Stage Separation Performance Analysis Project,” Final Report, H-34345D, Engineering Sciences, Inc., Huntsville, AL, 2002.
14. Wang, T.-S., Chen, Y.-S., Liu, J., Myrabo, L.N., and Mead, F.B. Jr., “Advanced Performance Modeling of Experimental Laser Lightcraft,” Journal of Propulsion and Power, Vol. 18, No. 6, 2002, pp. 1129-1138.
15. Wang, T.-S., “Multidimensional Unstructured-Grid Liquid Rocket Engine Nozzle Performance and Heat Transfer Analysis,” Journal of Propulsion and Power, Vol. 22, No. 1, 2005, pp. 78-84.
16. Wang, T.-S., “Transient 3-D Analysis of Nozzle Side Load in Regeneratively Cooled Engines,” AIAA Paper 2005-3942, 41st

AIAA/ASME/SAE/ASEE Joint Propulsion Conference, Tucson, Arizona, 2005.

17. Chen, Y.-S., and Kim, S. W., “Computation of Turbulent Flows Using an Extended k-ε Turbulence Closure Model,” NASA CR-179204, 1987.
18. Wang, T.-S., “Thermophysics Characterization of Kerosene Combustion,” Journal of Thermophysics and Heat Transfer, Vol. 15, No. 2, 2001, pp.140-147.
19. Uyehara, O.A., and Watson, K.M., "A Universal Viscosity Correlation," National Petroleum News, pp. R-714 to R-722, 1944.
20. Maxwell, J.B., Data Book on Hydrocarbons, Van Nostrand Co., NY, NY 1950.
21. Farmer, R.C., Cheng, G.C., and Chen, Y.S., “Parallel Processing of the 3D3P Codes,” SECA-FR-02-02, SECA, Inc., Huntsville, AL, 2002.
22. Dooley, R.B., Sec., "The International Association for the Properties of Water and Steam," September 1997 Release. See also 2001 and 2003 Releases available on IAPWS web site; Anon., "ASME Steam Properties for Industrial Use," ASME Press, NY, NY, 1998.
23. Dean, L.E., and Shurley, L.A., "Characteristics of RP-1 Rocket Fuel," Aerojet General Corporation, Technical Report TCR-70, 1957.
24. Computational Transport Phenomena for Engineering Analyses, Farmer, Cheng, Chen and Pike, 2009, Taylor & Francis.
25. Y. S. Chen, T.H. Chou, B.R. Gu, J.S. Wu, Bill Wu, Y.Y. Lian, and Luke Yang, “Real-Fluid Combustion Modeling of Hybrid Rocket Motors,” International Conference on Fluid Dynamics 2010, Sendai, Japan, November 1-3, 2010.
26. Vukelich S. R., Jenkins J. E., Missile Datcom: “Aerodynamic Prediction of Conventional Missiles Using Component Build-Up Techniques”, AIAA-84-0388, 1984.
27. Thomas J. Sooy and Rebecca Z. Schmidt, Aerodynamic Predictions, Comparisons, and Validations Using Missile DATCOM (97) and Aeroprediction 98 (AP98), JOURNAL OF SPACECRAFT AND ROCKETS Vol. 42, No. 2, March–April 2005.
28. Pitts, W.C., Nielsen, J.N., and Kaattari, G.E., “Lift and Center of Pressure of Wing-Body-Tail Combinations at Subsonic, Transonic, and Supersonic Speeds,” NACA Report 1307, 1957
29. Jorgensen L. H., Prefiction of Static Aerodynamic Characteristics for Space-Shuttle-Like and Other Bodies at Angles of Attack From 0o to 180o, NASA TN D-6996, 1973.
30. Hemsch M. J., Nielsen J. N., Equivalent angle-of-attack method for estimating nonlinear aerodynamics of missile fins, JOURNAL OF SPACECRAFT AND ROCKETS vol.20 no.4 (356-362), 1983.
31. Mendenhall M. R., Tactical Missile Aerodynamics: Prediction Methodology, Progress in Astronautics and Aeronautics Series, V-142 Published by AIAA, 1992.
32. Hopkins E.J., Keener E.R. and Inouye M., An Evalution of Theories for predicting Turbulent Skin Friction and Heat Transfer on Flat Plates at Supersonic and Hypersonic Mach Numbers, AIAA Journal,Vol.9, No.6,Jan.1971,pp.993-1003.
33. Lamb J. Parker and Oberkampf William L., “Review and Development of Base Pressure and Base Heating Correlations in Supersonic Flow”, JSR, Vol. 32, No. 1.
34. Mauri Tanner, “Base Pressure in Supersonic Flow:Further Thoughts About a Theory”, AIAA Journal,Vol. 30, No. 2.
35. Wendt, B.J., "A Parametric Study of Vortices Shed from Airfoil Vortex Generators", AIAA Journal, Vol. 42, No. 11 (tentative), November 2004.
36. Dudek, J.C., “Empirical Model for Vane-Type Vortex Generators in a Navier-Stokes Code,” AIAA Journal, Vol. 44, No. 8, 2006, pp. 1779–1789.

國科會補助專題研究計畫成果報告自評表

請就研究內容與原計畫相符程度、達成預期目標情況、研究成果之學術或應用價值（簡要敘述成果所代表之意義、價值、影響或進一步發展之可能性）、是否適合在學術期刊發表或申請專利、主要發現或其他有關價值等，作一綜合評估。

1. 請就研究內容與原計畫相符程度、達成預期目標情況作一綜合評估

■達成目標

□ 未達成目標（請說明，以 100 字為限）

□ 實驗失敗

□ 因故實驗中斷

□ 其他原因

說明：

Journals:

1. **Y.-S. Chen***, T. H. Chou, B. R. Gu, **J.-S. Wu***, Bill Wu, Y. Y. Lian, Luke Yang, "Multiphysics Simulations of Rocket Engine Combustion," Computers & Fluids, Vol. 45, pp. 29 – 36, 2011. (Keynote speech at ParCFD 2010)
2. M.-H. Hu, **J.-S. Wu*** and Y.-S. Chen, "Development of a Parallelized 2D/2D-Axisymmetric Navier-Stokes Equation Solver for All-Speed Gas Flows," Computers & Fluids, Vol. 45, pp. 241 – 248, 2011.

Conference papers:

1. **Yen-Sen Chen***, T. H. Chou, B. R. Gu, **J.-S. Wu***, Bill Wu, Y. Y. Lian, Luke Yang, "Real-Fluid Combustion Modeling of Hybrid Rocket Motors, 7th International Conference on Flow Dynamics, Sendai, Japan, November 1-3, 2010.
2. **J.-S. Wu***, T-H. Chou, Y.-S. Chen, H.-W. Hu, M.-T. Ho, H.-P. Lin, T.-L. Chen, Mathew R. Smith, Bill Wu and Y.-Y. Lian, **"**University-Based Hybrid Sounding Rocket Research in Taiwan, " 28th International Symposium on Space Science and Technology, Okinawa, Japan, June 5-12, 2011. (Invited Speech)
3. T.-H. Chou, **J.-S. Wu***, Y.-S. Chen and G. Cheng, "Numerical Investigation of Flow Characteristics Past a Mixing Enhancer in a Single-Port Hybrid Combustion Chamber," Ninth International Conference on Flow Dynamics (ICFD2012), Sendai, Japan, September 19-21, 2012.
4. K.-M. Chuang, J.-W. Lin, **J.-S. Wu***, Gary Cheng and Yen-sen Chen, "Numerical and Experimental Study of Venturi Flow Meters for Nitrous Oxide," Ninth International Conference on Flow Dynamics (ICFD2012), Sendai, Japan, September 19-21, 2012.
5. Yen-Sen Chen*, T. H. Chou, **J. S. Wu**, G. Cheng, "Sounding Rocket Development with Hybrid Combustion Technology," Ninth International Conference on Flow Dynamics (ICFD2012), Sendai, Japan, September 19-21, 2012. (Invited Speech)
6. Yen-Sen Chen, B. Wu, T. H. Chou, **J. S. Wu**, Gary Cheng, "Numerical Investigation of a Dual Vortical Flow Hybrid Rocket Motor," Ninth International Conference on Flow Dynamics (ICFD2012), Sendai, Japan, September 19-21, 2012.
7. Y.-S. Chen*, T.-H. Chou and **J.-S. Wu**, "Combustion Investigation of Hybrid Rocket Propulsion" The 22nd National Conference on Combustion Science and Technology, Kaohsiung, Taiwan, April 21-22, 2012.

2. 研究成果在學術期刊發表或申請專利等情形： 論文：■已發表 □未發表之文稿 ■撰寫中 □無 專利：□已獲得 ■申請中 □無 技轉：□已技轉 □洽談中 □無 其他：（以 100 字為限）
3. 請依學術成就、技術創新、社會影響等方面，評估研究成果之學術或應用價值（簡要敘述成果所代表之意義、價值、影響或進一步發展之可能性）（以 500 字為限） The present study has performed proposed study in terms of numerical simulations and experiments for hybrid rocker propulsion and aerodynamics. Results will be used to develop a realistic hybrid rocket in the PI's group. Several intensive large-scale static-burn and flight tests based on some preliminary results obtained from this project will be performed in 2013 through 2014. In the future, our team will be devoted to develop a similar, but larger scale, hybrid rocket system which can fly up to 200 km in altitude and conduct important scientific experiments in LEO.